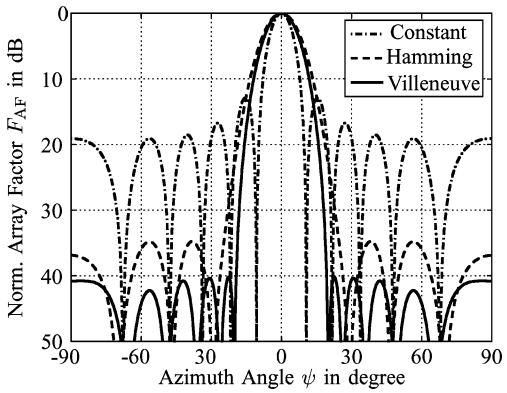

Fig. 5. Array factor of equivalent array. ($\Delta y_R = 0,6\lambda$, $N_{equv} = 9$).

TABLE IV
TAPER COEFFICIENT MATRIX ACCORDING TO TABLE III

0	Rx_1	Rx_2	Rx_3
Tx_1	0,1239	0,3451	0,6387
Tx_2	0,8981	1	0,8981
Tx_3	0,6387	0.3451	0.1239

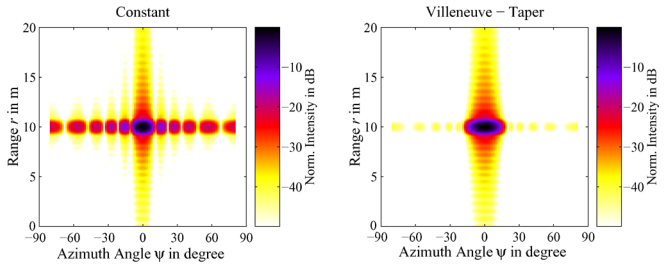

Fig. 6. Radar simulation of point target. ($\Delta y_R = 0,6\lambda$, $\Delta y_T = 1,8\lambda$, $M = 3$, $N = 3$, $B = 250$ MHz). (a) Constant taper. (b) Villeneuve taper.

array. The comparison shows that the chosen Villeneuve taper gives an even lower sidelobe level than the Hamming taper which does not reach the well-known sidelobe level of -43 dB since the number of elements is to small.

B. Matrix-Weighted Multitransmit DBF-Radar Simulation

The taper coefficient matrix is given in Table IV. Only for the center transmitter, the receiver taper is symmetric. For the transmitter at the left, the taper coefficients for the receivers are increasing and for the transmitter at the right, the coefficients are decreasing.

A Radar simulation of a point target has been performed. A multi transmit DBF system has been assumed with transmitter and receiver distribution as described in Fig. 3. In Fig. 6(a) the simulated Radar image is given for constant amplitude distribution. In this case the sidelobe level is -13 dB. In Fig. 6(b) the same simulation has been performed with a Villeneuve distribution leading to a broader main lobe but a lower sidelobe level.

This simulation example confirms the applicability a taper matrix to multitransmit DBF systems.

V. CONCLUSION

In this paper, the application of linear taper functions to multitransmit DBF systems is derived. It shows that multitransmit DBF can be considered by an equivalent receive-only array. Arbitrary taper functions can now be applied to them and be converted to matrix form for multitransmit DBF systems. This offers the great advantage, that beneficial taper functions can be applied to these sparse double-arrays, where conventional taper functions would fail.

REFERENCES

[1] S. W. Smith, H. G. Pavy, and O. T. von Ramm, "High-speed ultrasound volumetric imaging system. I. Transducer design and beam steering," *IEEE Trans. Ultrason., Ferroeletr., Freq. Control*, vol. 38, no. 2, pp. 100–108, Mar. 1991.
[2] M. Younis, "Digital beam-forming for high resolution wide swath real and synthetic aperture radar," Ph.D. dissertation, Forschungsberichte aus dem Institut für Höchstfrequenztechnik und Elektronik der Universität Karlsruhe, Germany, 2004.
[3] F. J. Harris, "On the use of windows for harmonic analysis with the discrete Fourier transform," *Proc. IEEE*, vol. 66, no. 1, pp. 51–83, Jan. 1978.
[4] A. H. Nuttall, "Some windows with very good sidelobe behavior," *IEEE Trans. Acoust., Speech Signal Process.*, vol. 29, no. 1, pp. 84–89, Feb. 1981.
[5] R. C. Hansen, *Phased Array Antennas*. New York: Wiley, 1997.
[6] C. Balanis, *Antenna Theory: Analysis and Design*. New York: Wiley, 1982.
[7] A. T. Villeneuve, "Taylor patterns for discrete arrays," *IEEE Trans. Antennas Propag.*, vol. 32, no. 10, pp. 1089–1093, Oct. 1984.
[8] D. A. McNamara, "Generalised Villeneuve $\bar{n}$ distribution," *Proc. Inst. Elect. Eng. Microwaves, Antennas and Propagation*, vol. 136, no. 3, pp. 245–249, Jun. 1989.

On a Class of Planar Absorbers With Periodic Square Resistive Patches

Hosung Choo, Hao Ling, and Charles S. Liang

***Abstract*—A Pareto genetic algorithm is used to explore the performance of planar absorbers incorporating a sheet of periodic resistive patches embedded in a primary material substrate. The absorbing performance of a single-layer electric radar absorbing material (eRAM) with periodic resistive patches is compared to that of standard dual-layer absorbers made of wax laid on top of eRAM or magnetic radar absorbing material (mag-RAM).**

***Index Terms*—Pareto genetic algorithm, periodic resistive patches, planar absorbers.**

I. INTRODUCTION

The practical application of radar absorbers on aerospace vehicles can broadly be categorized into radar absorbing structures (RAS) [1], [2] and radar absorbing materials (RAM). RAS are primarily made of cellular core materials (loaded core or sandwiched loaded sheets) designed to handle partial structural load and are generally less than

Manuscript received July 10, 2006; revised January 9, 2008. Published July 7, 2008 (projected). This work was supported in part by the Office of Naval Research under Contract N00014-01-1-0224, in part by the Texas Higher Education Coordinating Board under the Texas Advanced Technology Program, and in part by the National Science Foundation Major Research Instrumentation Program.

H. Choo is with the School of Electronic and Electrical Engineering, Hongik University, Seoul, Korea (e-mail: hschoo@hiongik.ac.kr).
H. Ling is with the Department of Electrical Engineering, The University of Texas at Austin, Austin, TX 78712 USA.
C. S. Liang is with Lockheed Martin Aeronautics Company, Fort Worth, TX 76101 USA.

Color versions of one or more of the figures in this paper are available online at http://ieeexplore.ieee.org.
Digital Object Identifier 10.1109/TAP.2008.924766

0018-926X/$25.00 © 2008 IEEE

Authorized licensed use limited to: HONGIK UNIVERSITY. Downloaded on January 12, 2010 at 20:57 from IEEE Xplore. Restrictions apply.

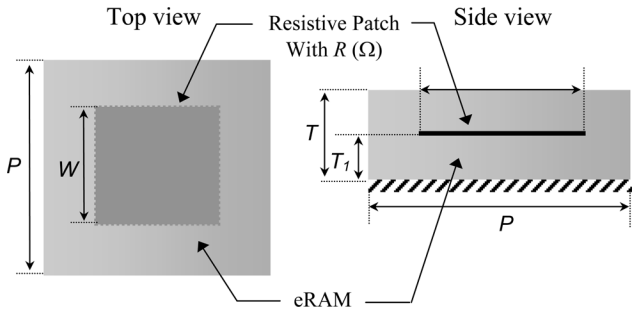

Fig. 1. Geometry of a planar absorber with embedded periodic resistive patches.

50 mm thick for flat-panel usage. On the other hand, RAM are thin coatings of structurally parasitic absorbing materials generally less than 6.5 mm in thickness. They are preferred for use due to their lower volume, lighter weight, and minimal structural impact, provided the design can meet the required electrical performance. Thus far, multilayered RAM designs have been confined to academic interest due to difficulties in developing materials with suitable electrical and mechanical properties and lack of robust manufacturing techniques to assemble dissimilar materials. In general, dual-layer designs are considered only if broadband and wide angular electrical performances are essential.

Recently, Terracher and Berginc [3] proposed a method to simultaneously lower the operating frequency and broaden the bandwidth of a single-layer, non-magnetic eRAM absorber. Their design entails placing periodic, perfectly conducting (PEC), square patches on the top surface of a planar eRAM. Even though the lossy dielectric material used is a rather poor stand-alone absorber, the layer of periodic metallic patches dramatically improves the performance of the combination to a respectable level. The objective of this Communication is to explore whether their design can be further optimized and generalized such that the resultant performance can nearly match that of a dual-layer magnetic RAM (magRAM). If so, then the design may potentially be easier to implement in practice than the dual-layer magRAM.

The use of genetic algorithms (GAs) in the design of multilayered planar absorber structures has been extensively studied [4]–[7]. Corrugated coatings with periodic non-planar shape profiles offer additional degrees of design freedom, and GA-optimized non-planar coating structures have been also reported by the authors [8]. In this paper, the Pareto GA coupled with a full-wave electromagnetic solver is used to design low-profile planar periodic absorber for broadband and wide angular operations. First, the optimal set of designs on the Pareto front are found for the patch absorbers used in [3] by trading off coating thickness and absorbing characteristics. Then, the designs are further refined by exploring additional degrees of freedom including the patch resistivity, size, period, and its height within the substrate. Finally, the performances of the optimized designs are compared against results obtained from the standard dual-layered absorber designs. Several GA optimized designs with different thickness are shown, and the physical interpretations of the resultant performance are also discussed.

II. Pareto GA Optimization

The geometry considered is shown in Fig. 1. The absorber consists of a single layer of lossy material backed by a perfectly conducting ground-plane. Planar square resistive patches are embedded periodically inside the lossy material. The incident wave direction is defined as θ measured from normal to the substrate. The design parameters are the coating thickness (T) and the patch size (W), resistivity (R), period (P), and height above ground-plane (T_1). A Pareto GA is implemented to search for the optimal design parameters for achieving

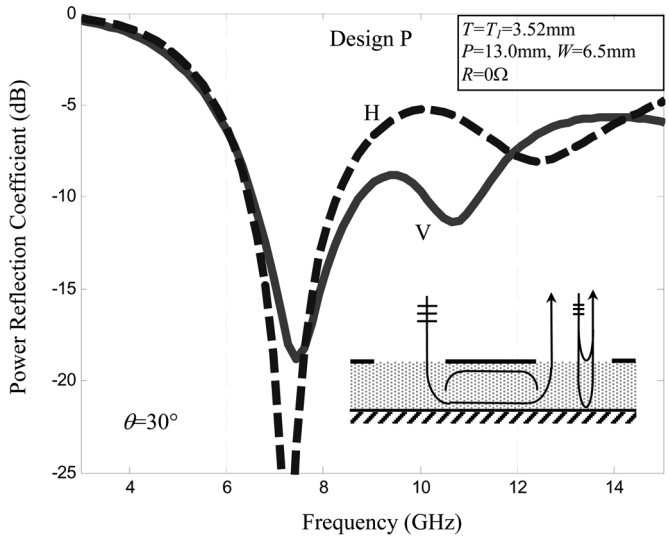

Fig. 2. Absorption performance of design P with top-mounted PEC patches at $\theta = 30^\circ$. Vertical polarization (_____). Horizontal polarization (- - - - -).

two critical design objectives: low profile and good absorption performance. The two costs associated with the design goals are

$$\text{Cost } 1 = \text{Absorber coating thickness } (T)$$

$$\text{Cost } 2 = \text{Average power reflection coefficient}$$

$$\frac{1}{2N}\sum_{f,\theta}^{N}\left(|\Gamma_{\perp}|^2 + |\Gamma_{||}|^2\right) \tag{1}$$

where the Γ's represent the field reflection coefficients for the perpendicular and parallel polarized incident waves within the frequency-angular range of interest. It is worthwhile pointing out that other cost definitions (such as minimax) for Cost2 can also be used. This issue was examined previously in [8]. The results did not show significant differences among the various cost definitions. The present designs are confined within the frequency band of $f = 6$ to 12 GHz and the angular region of $\theta = 30^\circ$ to 60°. After evaluating the cost functions of each sample structure using a full-wave periodic patch code [9], all the samples of the population are ranked using the non-dominated sorting method. Then, a reproduction process is performed to refine the population into the next generation based on their rank. In order to prevent solutions from converging to a single point, the sharing scheme described in [10] is used to generate a well-dispersed population. The final converged "Pareto front" contains those absorber designs that are optimal in at least one of the two objectives.

III. Results

The Pareto GA process described above is first applied to find the optimal design parameters when the PEC patch $(R = 0\Omega)$ is restricted to the top of the eRAM $(T_1 = T)$, as was done in [3]. The same lossy eRAM material as in [3] (with a dielectric constant of approximately 5-j1.6) is used for the coating material. Fig. 2 shows a representative optimized design (marked as Design P in Fig. 3) and its spectral absorption performance for $\theta = 30^\circ$. There are two dips in the absorption curve for each polarization (located at 7.5 and 10.5 GHz for V and at 7.5 and 12.5 GHz for H). These are caused by, respectively, the patch absorption resonance (due to energy trapped beneath the patch) and the standard front-back destructive interference of the exposed dielectric slab. These two mechanisms are illustrated in the inset of Fig. 2. The overall converged Pareto front with the above design constraints is shown in Fig. 3 as "×." It is noted that rank-one solutions

Authorized licensed use limited to: HONGIK UNIVERSITY. Downloaded on January 12, 2010 at 20:57 from IEEE Xplore. Restrictions apply.

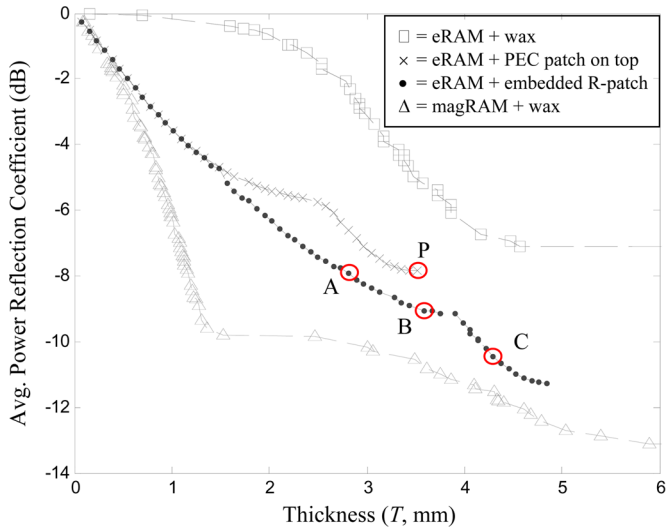

Fig. 3. Optimized absorption performance vs. absorber thickness. Dual-layer coating with eRAM and wax (□). eRAM with top-mounted PEC patches (×). eRAM with embedded resistive patches (•). Dual-layer coating with magRAM and wax (Δ).

can achieve an average power reflection coefficient down to -7.9 dB at $T = 3.52$ mm. For comparison, the Pareto front for dual-layer absorbers with no patch is also generated via the Pareto GA and plotted as "□" in Fig. 3. These dual-layer designs consist of wax (with a dielectric constant of about 2.4-j0.08) over eRAM. Clearly, the single-layer eRAM with patches is thinner and has superior absorption performance than the reference dual-layer design.

To further improve on the absorption performance, the design is next allowed two additional degrees of freedom: (1) placement of the patch inside the absorber ($T_1 \leq T$), and (2) variable patch resistivity ($0 \leq R \leq 1{,}200\,\Omega$). The new design freedom resulted in a further improved Pareto front shown as dots in Fig. 3. The average power reflection coefficient can be decreased to -11.26 dB at $T = 4.84$ mm. It is interesting to note that no noticeable performance improvement is achieved initially for thickness $T < 1.4$ mm. However, significant improvements can be obtained when the thickness is increased beyond this point due to the additional design freedoms (details will be discussed later). For comparison, the Pareto front of an optimized dual-layer design of wax-covered magRAM is also generated and plotted as "Δ" in Fig. 3. It is important to note that, with sufficient thickness, the performance of the single-layer eRAM with patches can nearly approach that of the dual-layer magRAM absorber. The weight penalty of the magRAM and the material bonding issue associated with any dual-layer structure makes the eRAM with patches a potential alternative.

Next, let us examine the absorption physics of the optimized eRAM absorber with patches. The detailed design parameters are plotted in Fig. 4 for the optimized absorber configurations. The patch size (W) and period (P) are plotted versus absorber thickness (T) in Fig. 4(a); and Fig. 4(b) shows the patch height (T_1) over ground-plane and the patch resistivity (R) versus absorber thickness. A sudden change in the patch size and patch period is clearly observed in Fig. 4(a) at the absorber thickness of 3.2 mm. From Fig. 4(b), we also observe that the optimal patch position moves from the top of the absorber to inside the absorber when the absorber thickness exceeds 3.8 mm. Therefore, three distinct classes of optimized designs for $T \leq 3.2$ mm, $3.2\text{ mm} \leq T \leq 3.8$ mm and $T \geq 3.8$ mm are noted. To examine the operating physics of the designs in more detail, three specific optimized designs (labeled as A, B and C) are selected for discussion. For design A ($T = T_1 = 2.81\,\text{mm}, P = 4.41\,\text{mm}, W = 3.86\,\text{mm}, R = 114\Omega$),

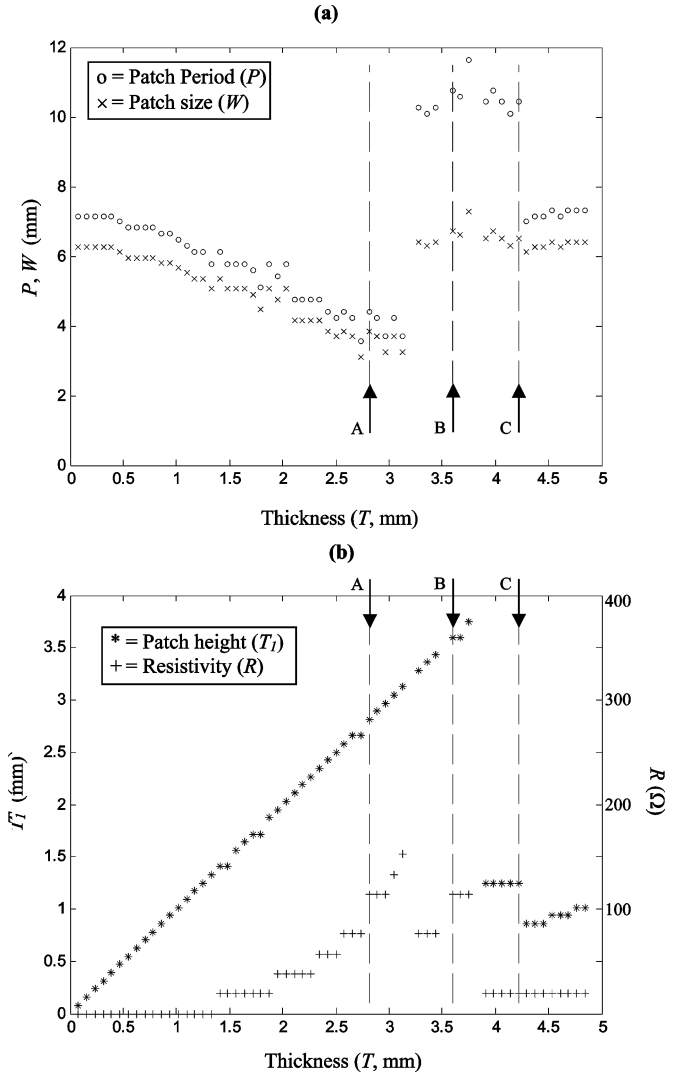

Fig. 4. (a) Optimized patch size and period versus thickness. (b) Optimized patch height and patch resistivity versus thickness.

the resistive patches are located on top of the coating, and the gaps between the patches are physically small ($P - W = 0.55$ mm). In this case, the patch resonance produces good absorbing characteristics. This effect occurs when the patch size is on the order of half a wavelength in the material. The patch resonance is affected more by its own resistivity than its height within the substrate. The larger the patch height, the broader the resonance dip and the lower the resonant frequency due to fringing effects of the resonant field. For design B ($T = T_1 = 3.59$ mm, $P = 10.77$ mm, $W = 6.73$ mm, $R = 114\,\Omega$), the patch is still located on top of the coating. Both the patch size and the patch period increase significantly as compared to design A. In this case, the patch resonance is lowered compared to design A due the much larger patch size. However, since there is now a larger gap between neighboring patches ($P - W = 4.04$ mm), an additional destructive interference dip due to the exposed ground-plane backed dielectric is created. This situation is similar to what was shown in Fig. 2 for design P. For design C ($T = 4.22$ mm, $T_1 = 1.25$ mm, $P = 10.42$ mm, $W = 6.51$ mm, $R = 19\,\Omega$), the patch is embedded inside the eRAM slab. Fig. 5 shows the spectral absorption performance for $\theta = 30^\circ$ of this design. Interestingly, this design achieves the desirable broadband response over the frequency range of interest by being able to have three separate resonances. First, the patch resonance

Authorized licensed use limited to: HONGIK UNIVERSITY. Downloaded on January 12, 2010 at 20:57 from IEEE Xplore. Restrictions apply.

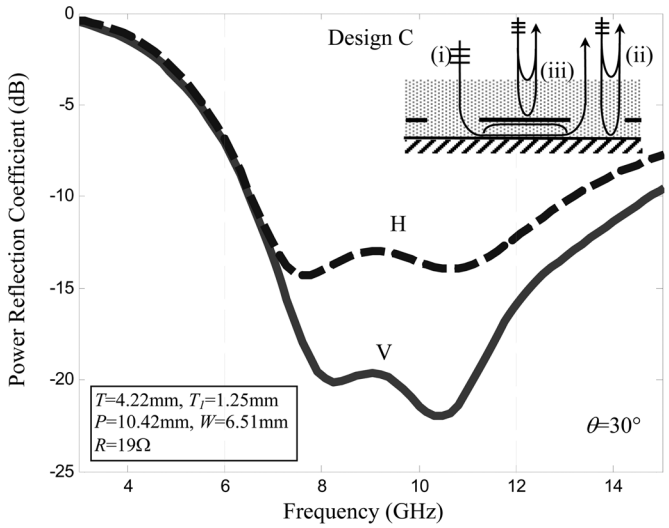

Fig. 5. Absorption performance of design C with embedded resistive patches at $\theta = 30°$. Vertical polarization (_____). Horizontal polarization (- - - - -).

occurs at a frequency around 8 GHz. Second, the exposed gaps between the patches create a conventional planar absorber that produces a resonance at 11 GHz. Third, the patches themselves serve as an additional ground plane to create a thinner planar absorber to enhance performance above 11 GHz. The three mechanisms are illustrated in the inset of Fig. 5 and labeled as (i), (ii), and (iii). These effects combine to allow eRAM with periodic resistive patches to exhibit absorbing characteristics comparable to those of a dual-layer magRAM.

IV. Conclusion

A Pareto genetic algorithm has been applied to design planar absorbers with periodic resistive patches in terms of absorption performance and absorber thickness. The performance of a single-layer eRAM absorber incorporating a resistive patch array can be made comparable to that of a dual-layer magRAM. Three specific designs were selected from the Pareto front to illustrate the different optimization regimes and to investigate the operating principles of each. The best broadband absorbing characteristics are achieved by strong resonance of patches placed near ground as well as by the destructive interference phenomena occurring in the coated patch array and the coated ground-plane.

References

[1] R. L. Fante and M. T. McCormack, "Reflection properties of the Salisbury screen," *IEEE Trans. Antennas Propag.*, vol. 36, pp. 1443–1454, Oct. 1988.
[2] E. C. Smith, "Design principles of broadband adaptive Salisbury screen absorber," *Electron. Lett.*, vol. 38, pp. 1052–1054, Aug. 2002.
[3] F. Terracher and G. Berginc, "A broadband dielectric microwave absorber with periodic metallizations," *J. Electromagn. Waves Applicat.*, vol. 13, pp. 1725–1741, Dec. 1999.
[4] D. Weile, E. Michielssen, and D. E. Goldberg, "Genetic algorithm design of Pareto optimal broadband microwave absorbers," *IEEE Trans. Electromagn. Compat.*, vol. 38, pp. 518–525, Aug. 1996.
[5] S. Chakravarty, R. Mittra, and N. R. Williams, "Application of a microgenetic algorithm (MGA) to the design of broadband microwave absorbers using multiple frequency selective surface screens buried in dielectrics," *IEEE Trans. Antennas Propag.*, vol. 50, pp. 284–296, Mar. 2002.
[6] D. J. Kern and D. H. Werner, "A genetic algorithm approach to the design of ultra-thin electromagnetic bandgap absorbers," *Microw. Opt. Tech. Lett.*, vol. 38, pp. 61–64, May 2003.
[7] S. Cui, D. S. Weile, and J. L. Volakis, "Noel planar electromagnetic absorber designs using genetic algorithms," *IEEE Trans. Antennas Propag.*, vol. 54, pp. 1811–1817, Jun. 2006.
[8] H. Choo, H. Ling, and C. S. Liang, "Shape optimization of corrugated coatings under grazing incidence using a genetic algorithm," *IEEE Trans. Antennas Propag.*, vol. 51, pp. 3080–3087, Nov. 2003.
[9] H. Ling, S. Han, L. C. Trintinalia, and H. Choo, "CoatFSS, 3D Scattering from Layer Coatings with Embedded Metal or R-card Patches, Version 2.0," Aug. 2002.
[10] J. Horn, N. Nafpliotis, and D. E. Goldberg, "A niched Pareto genetic algorithm for multi-objective optimization," in *Proc. 1st IEEE Conf. on Evolutionary Computation*, 1994, vol. 1, pp. 82–87.

Acceleration of the Method of Moments Calculations by Using Graphics Processing Units

Shaoxin Peng and Zaiping Nie

***Abstract*—The graphics processing unit (GPU) has been used to speed up the conventional method of moments (MoM) calculations for electromagnetic scattering from arbitrary three-dimensional conducting objects. The acceleration ratio of filling impedance matrix has reached 30, while the total acceleration ratio (including iteration) is about 20. Moreover, a matrix splitting algorithm is developed to break up the texture limit. It splits the huge matrix into multiple, tiny matrixes, each of which can be fit into one texture. Then, the system memory can be used to store all the elements of the impedance matrix, making it possible to deal with electrically large problems, since the capacity of video card's memory is no longer a limit.**

***Index Terms*—Graphics processing unit (GPU), hardware speed-up, matrix splitting algorithm, method of moments (MoM), numerical solution.**

I. Introduction

Recently, the graphics processing unit (GPU) has become a prevalent commodity in personal computers. The computational capability of GPU has outstripped that of conventional central processing unit (CPU). For example, the Intel 3 GHz Pentium 4 processor has reached 6×10^9 floating point operations per second (FLOPS) theoretically, whereas the NVIDIA GeForce 6800 Ultra graphics processor has reached 40×10^9 FLOPS as observed in [1]. This strong computational power mainly owes to the parallelism of GPUs' multiple vertex and fragment pipelines, as well as the ability to execute a four-dimensional vector operation within a single instruction. In addition, the high memory bandwidth of GPU also contributes to its performance [1].

Originally designed for graphics rendering tasks, the GPU is also proved to be very effective for massively parallel vector math operations. The high performance of GPU has been reported in many applications, such as audio and signal processing, image processing and volume rendering [2]. These achievements have demonstrated the potential power of GPU in the field of scientific computation.

The application of GPU in the area of computational electromagetics started in the finite-difference time-domain method (FDTD). Kraki-

Manuscript received December 5, 2006; revised August 22, 2007. Published July 7, 2008 (projected). This work was supported in part by the National Science Foundation of China under Contract 60571022, in part by the Innovative Research Team Program of UESTC, China, and in part by the 111 Project (No. B07047).

The authors are with the Electronic Engineering Department, University of Electronic and Science Technology of China, Chengdu 610054, China (e-mail: sxpeng@uestc.edu.cn, zpnie@uestc.edu.cn).

Digital Object Identifier 10.1109/TAP.2008.924768

0018-926X/$25.00 © 2008 IEEE

Authorized licensed use limited to: HONGIK UNIVERSITY. Downloaded on January 12, 2010 at 20:57 from IEEE Xplore. Restrictions apply.